OPEN ACCESS

A comprehensive framework for fluorescence cross-correlation spectroscopy

To cite this article: Jonas Ries *et al* 2010 *New J. Phys.* **12** 113009

New Journal of Physics
The open-access journal for physics

A comprehensive framework for fluorescence cross-correlation spectroscopy

Jonas Ries[1,2], **Zdeněk Petrášek**[1], **Anna J García-Sáez**[1,3] **and Petra Schwille**[1,4,5]

[1] Biotechnologisches Zentrum, TU Dresden, Tatzberg 47-51, 01307 Dresden, Germany
[2] ETH Zürich, LPC, Wolfgang-Pauli-Strasse 10, 8093 Zürich, Switzerland
[3] BIOQUANT, Im Neuenheimer Feld 267, 69120 Heidelberg, Germany
[4] Max-Planck-Institute for Molecular Cell Biology and Genetics, Pfotenhauerstrasse 108, 01307 Dresden, Germany
E-mail: petra.schwille@biotec.tu-dresden.de

New Journal of Physics **12** (2010) 113009 (32pp)
Received 17 May 2010
Published 4 November 2010
Online at http://www.njp.org/
doi:10.1088/1367-2630/12/11/113009

Abstract. Dual-colour fluorescence cross-correlation spectroscopy is a powerful method of studying binding between labelled biomolecules *in vitro* as well as *in vivo*. However, numerous artefacts and experimental complexities complicate quantitative measurements. Here, we show that a combination of dual-colour fluorescence correlation spectroscopy (FCS) with dual-focus FCS avoids artefacts due to chromatic aberrations or saturation and circumvents the calibration of the detection volumes. In addition, we present a comprehensive mathematical framework that allows us to accurately analyse correlation curves even in the presence of spectral cross-talk, incomplete or stochastic labelling, multiple binding sites, a fluorescent background and depletion due to photobleaching. We demonstrate the merits of this approach using dual-colour dual-focus scanning FCS, which allows binding measurements on membranes not affected by membrane movements.

[5] Author to whom any correspondence should be addressed.

Contents

1. Introduction

Biological processes depend on concentrations, mobilities and interactions of biomolecules. A powerful technique for measuring these parameters is fluorescence correlation spectroscopy (FCS). It is based on the statistical analysis of intensity fluctuations of fluorescent molecules diffusing through a sub-micrometre detection volume. From the auto-correlation of the fluorescence signal, diffusion coefficients and concentrations can be estimated if the geometry of the detection volume is known. In dual-colour fluorescence cross-correlation spectroscopy (FCCS) [1], an extension of FCS, the cross-correlation of intensity fluctuations in two spectral channels allows determination of the degree of binding between two differently labelled species.

The introduction of commercial confocal FCS systems has promoted the use of FCS so that it can now be considered a well-established technique for *in vitro* as well as *in vivo* studies [2]–[7]. However, standard FCS suffers from several limitations, especially in complex biological systems, which limit its applicability. The main experimental challenges are summarized in table 1. Optical artefacts [7, 8], such as varying cover slide thickness, refractive index mismatch, optical saturation or aberrations, change the size of the detection volume, thereby precluding precise calibration necessary for quantitative measurements. Dual-focus FCS [9, 10] and circle-scanning FCS [11] overcome this problem for single-colour FCS by using two spatially distinct detection volumes or a well-defined scan path. In these methods, the knowledge of the distance between the detection volumes, or the scan radius, replaces the calibration of the volume size.

Quantitative binding studies are especially challenging. The exact geometries of the two spectrally distinct detection volumes (henceforth referred to as red and green) are difficult to calibrate. This is particularly true for the displacement between the red and the green detection volumes due to chromatic aberrations. Furthermore, the spectral cross-talk, usually from the green fluorophore into the red channel, leads to false positive cross-correlation. Finally, labelling efficiencies and binding stoichiometries affect the correlation amplitudes and have to be taken into account during data analysis.

Förster (or fluorescence) energy transfer (FRET) is an alternative method to probe molecular interactions [12]–[14]. Here, the energy transfer from the first excited electronic state of the donor to the acceptor is used to determine the proximity of the two molecules. In contrast to FCS, FRET is not restricted to mobile molecules at low concentrations and allows investigation of conformational changes and binding geometries. On the other hand, FRET requires a thorough choice of donor and acceptor fluorophores at specific positions in the molecular complex; and quantitative measurements of binding affinities are difficult due to the numerous parameters that influence the measured FRET efficiencies.

In this paper, we aim to overcome the problem of the calibration of the size of the measurement volume in dual-colour FCS by combining this technique with dual-focus FCS. This is accomplished by measurement of intensity fluctuations in four channels, resulting from a combination of two spatially distinct detection volumes in two spectral channels, and simultaneous analysis of all spatial and spectral correlation curves, thus enabling quantitative binding studies without calibration of the exact geometry of the detection volumes. We demonstrate the feasibility of simultaneous dual-colour dual-focus FCS on artificial membranes by using a scanning FCS approach [10] with the additional advantage of being insensitive to membrane movements. Compared to previous dual-colour scanning FCS applications [6, 15],

Table 1. Artefacts in dual-colour cross-correlation spectroscopy.

Problem	Resulting error	Solution
Imperfect overlap of red and green detection volume	Underestimation of complex concentration C_{ab}	• Simultaneous dual-focus dual-colour cross-correlation spectroscopy • Careful calibration
Different sizes of red and green detection volumes	Wrong concentrations C_a, C_b, C_{ab}	
Size of red and green detection volumes not precisely determined		
Optical saturation		
Fluorescent background	Underestimation of complex concentration C_{ab}, overestimation of monomer concentrations C_a, C_b	Correct the amplitudes of correlation curves
Spectral cross-talk	Overestimation of complex concentration C_{ab}, false-positive binding	• Alternating excitation • Take cross-talk into account during data fitting (tables 3, 5 and 6)
Triplet	Additional fast kinetics	Take into account during data fitting (tables 3, 5 and 6)
Incomplete labelling	Underestimation of concentrations C_a, C_b, C_{ab}	
Multiple stochastic labelling	Wrong concentrations	
Multiple binding sites		
Depletion due to photobleaching	• Distortions of correlation curves • Wrong concentrations • False-positive or false-negative binding	Correction of intensity traces prior to calculating correlation curves
External instabilities		
Bleaching of background		
Membrane movements	Overestimation of complex concentration or false-positive binding	Scanning FCS
Photobleaching	Errors in diffusion coefficients and concentrations	Reduction of excitation intensity
Fluorescence quenching	Error in concentrations	Take into account during data fitting
Single bright events	Distortions of correlation curves	• Hand-selection of uncorrupted curves • Automatic selection of curves

here the additional analysis of the dual-colour dual-focus cross-correlation curve overcomes the need for calibrating the overlap between the red and the green detection volume.

In addition, we present a comprehensive mathematical framework to fit the experimental data, taking into account most experimental complexities such as spectral cross-talk, incomplete labelling, statistical labelling, multiple binding sites, a fluorescent background, blinking/triplet dynamics or slow variations of the intensity caused e.g. by depletion due to photobleaching. By reducing the number of additional parameters to a minimum, this framework extends the use of FCS to complex systems. It is not restricted to dual-colour FCS but will be useful for FCS or image correlation spectroscopy (ICS [16, 17]) in general.

2. Theoretical description of fluorescence correlation spectroscopy (FCS)

2.1. The auto-correlation curve

In FCS, fluorescence fluctuations due to molecules moving through a tiny (sub-femtolitre) detection volume are analysed statistically in terms of the experimental auto-correlation curve $\tilde{G}(\tau)$ (figures 1(a) and (b)):

$$\tilde{G}(\tau) = \frac{\langle \delta F(t) \delta F(t+\tau) \rangle}{\langle F(t) \rangle^2} = \frac{\tilde{g}(\tau)}{\langle F(t) \rangle^2}, \tag{1}$$

where $F(t)$ is the fluorescence intensity, $\langle\rangle$ denotes the average over time and $\delta F(t) = F(t) - \langle F(t) \rangle$. $\tilde{g}(\tau)$ is the non-normalized auto-correlation curve.

The shape of the correlation curves is determined by dynamic processes causing the fluctuations (e.g. diffusion of the fluorescent molecules through the detection volume) and the geometry of detection volume. To extract the parameters of interest (e.g. concentrations and diffusion coefficients), the experimental correlation curve is fitted with a mathematical model describing the fluctuations (correlation function $G(\tau)$). In the following, we derive such mathematical models to fit experimental correlation curves under realistic conditions, taking into account most experimental complexities. The experimentally determined, derived and theoretical quantities, as well as the parameters, divided into setup-related and sample-related, are summarized in table 2. The setup-related parameters are either pre-determined by calibration measurements or treated as free parameters and determined by data fitting if difficult to determine independently. We are primarily interested in the sample-related parameters, such as diffusion coefficients or concentrations, which are determined by fitting. Care was taken that the number of free fitting parameters is minimal, that they can directly be related to absolute physical quantities and that all parameters can be determined experimentally.

The most basic model describing the diffusion of a molecule with diffusion coefficient D and concentration C through a three-dimensional (3D) Gaussian detection volume of radial dimension w and axial dimension $w_z = Sw$ (aspect ratio S) is

$$\begin{aligned} G(\tau) &= \frac{1}{C} \frac{1}{\pi^{3/2} w^2 w_z} \left(1 + \frac{4D\tau}{w^2}\right)^{-1} \left(1 + \frac{4D\tau}{w_z^2}\right)^{-1/2} \\ &= \frac{1}{N} \left(1 + \frac{\tau}{\tau_D}\right)^{-1} \left(1 + \frac{\tau}{\tau_D S^2}\right)^{-1/2}, \end{aligned} \tag{2}$$

where $N = CV$ is the average number of particles in the detection volume $V = \pi^{3/2} w^2 w_z$ and $\tau_D = w^2/4D$ is the diffusion time.

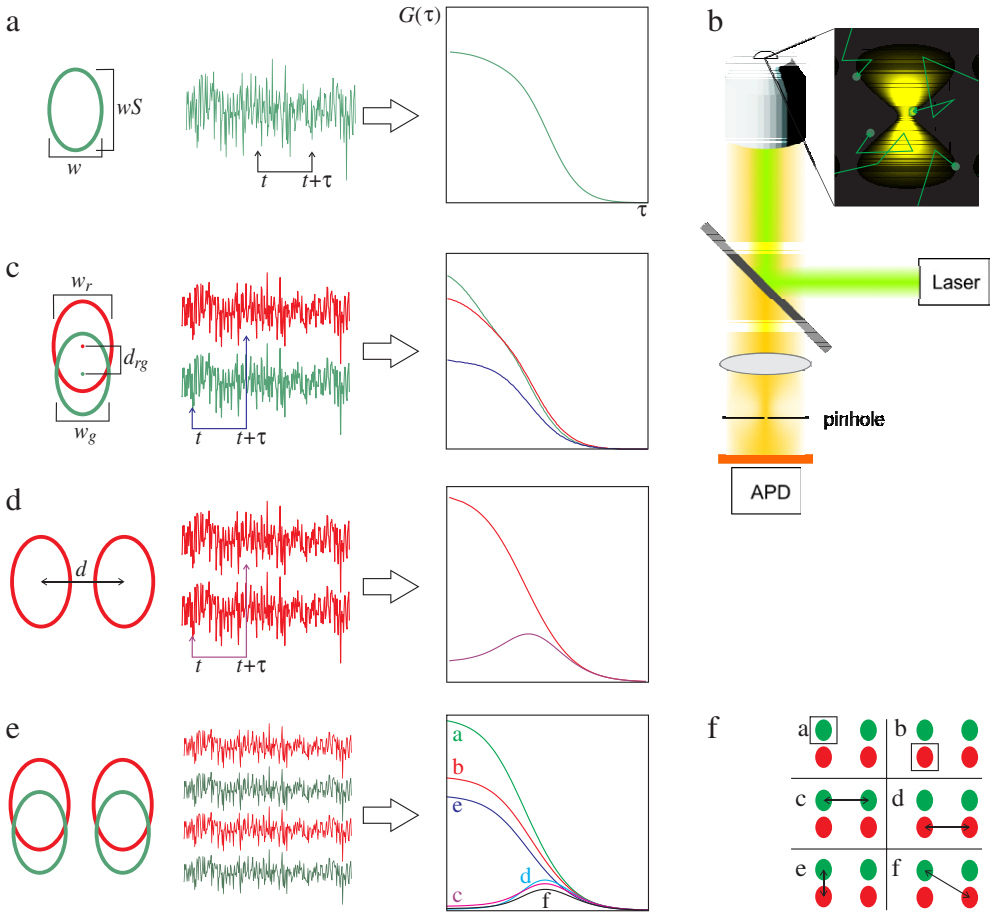

Figure 1. Overview of different fluorescence correlation spectroscopy methods. (a) The principle of FCS. Fluorescent molecules diffusing through the detection volume give rise to a fluctuating intensity. The auto-correlation curve measures the self-similarity of these fluctuations and can be used to infer e.g. concentrations and diffusion coefficients. w denotes radial dimension ($1/e^2$-radius) of the Gaussian detection profile, and $S = w_z/w_{x,y}$ is the aspect ratio. (b) Schematic of the confocal setup used for FCS. (c) Dual-colour cross-correlation. The cross-correlation curve compares the intensity fluctuations in the red and the green channel and can be used to quantify binding between red and green molecules. The dimensions of the red and green detection volumes, w_r and w_g, respectively, can be different; also the detection volumes might be offset by d_rg due to chromatic aberrations. (d) Dual-focus cross-correlation does not rely on a calibration of the detection volume if the distance d between the two detection volumes is known. (e) Combining dual-colour FCS with dual-focus FCS results in four different fluctuating intensities from which 16 correlation curves can be calculated. In the absence of directed motion only six are distinct (f): two autocorrelations of the green[a] and the red[b] species, respectively; two spatial cross-correlations of the green[c] and the red[d] species, respectively; and two cross-correlations between the two colours, one at the same position[e] and the other between two different position[f].

Table 2. Overview of the parameters used in this paper.

(a): Experimental (measured) quantities	
$\tilde{G}^{11}_{rr}(\tau) = \tilde{G}^{22}_{rr}$	Red auto-correlation
$\tilde{G}^{11}_{gg}(\tau) = \tilde{G}^{22}_{gg}$	Green auto-correlation
$\tilde{G}^{12}_{rr}(\tau) = \tilde{G}^{21}_{rr}$	Red dual-focus cross-correlation
$\tilde{G}^{12}_{gg}(\tau) = \tilde{G}^{21}_{gg}$	Green dual-focus cross-correlation
$\tilde{G}^{11}_{rg}(\tau) = \tilde{G}^{22}_{rg} = \tilde{G}^{11}_{gr} = \tilde{G}^{22}_{gr}$	Dual-colour cross-correlation
$\tilde{G}^{12}_{rg}(\tau) = \tilde{G}^{21}_{rg} = \tilde{G}^{12}_{gr} = \tilde{G}^{21}_{gr}$	Dual-colour dual-focus cross-correlation
$\tilde{g}^{\cdot\cdot}_{\cdot\cdot}(\tau)$	Non-normalized correlations corresponding to $\tilde{G}^{\cdot\cdot}_{\cdot\cdot}(\tau)$
$F_r(t)$, $F_g(t)$	Fluorescence intensities
$\langle \mathrm{Fr}(t)\rangle$, $\langle F_g(t)\rangle$	Mean measured fluorescence intensities including background
B_r,B_g	Background
(b): Derived quantities	
F^m_r, F^m_g	Experimental background-corrected mean intensities
F_r, F_g	Mathematical expression for mean intensities
g_{rr}, g_{gg}, g_{rg}	Non-normalized correlation functions
g^a_{rr}, g^b_{gg}, g^{ab}_{rg}, g^{ab}_{rr},...	Single-species correlation functions (species a, b, complex ab)
$g^{\cdot\cdot}_{\cdot\cdot}(\tau)$, $G^{\cdot\cdot}_{\cdot\cdot}(\tau)$	Theoretical correlations (models) corresponding to $\tilde{g}^{\cdot\cdot}_{\cdot\cdot}(\tau)$, $\tilde{G}^{\cdot\cdot}_{\cdot\cdot}(\tau)$
(c): Setup-related parameters	
d	Lateral distance between two foci
w_r, w_g, S_r, S_g	Lateral dimensions and aspect ratios of detection volumes
d_{rg}	Axial displacement of detection volumes due to chromatic aberrations
κ	Cross-talk coefficient from the green fluorophore in the red channel (15)
η_r, η_g	Channel brightnesses (9)
(d): Sample-related parameters	
C_a, C_b, C_{ab}	Concentrations
D_a, D_b, D_{ab}	Diffusion coefficients
f_T, τ_t	Triplet/blinking fraction and the corresponding time constant

2.2. Dual-colour cross-correlation

To measure binding between two distinctly labelled molecules, dual-colour FCS (figure 1(c)) can be employed. Here, two spectral channels are used to calculate the auto-correlation curves $\tilde{G}_r(\tau)$, $\tilde{G}_g(\tau)$ (1) and also the spectral cross-correlation curve $\tilde{G}_{rg}(\tau)$ from the intensity traces $F_r(t)$ and $F_g(t)$ in the red and green channels, respectively:

$$\tilde{G}_{rg}(\tau) = \frac{\langle \delta F_r(t)\delta F_g(t+\tau)\rangle}{\langle F_r(t)\rangle\langle F_g(t)\rangle} = \frac{\tilde{g}_{rg}(\tau)}{\langle F_r(t)\rangle\langle F_g(t)\rangle}. \tag{3}$$

Only if the two binding partners diffuse as a single entity do they give rise to a significant cross-correlation amplitude, which can then be used to infer the degree of binding. Analysis of auto- and cross-correlation curves allows determination of concentrations of the binding partners C_a and C_b and the concentration C_{ab} of the complex. For a simple binding reaction $A + B \rightleftharpoons AB$ the dissociation constant K_D follows directly from the measured concentrations:

$$K_D = \frac{C_a C_b}{C_{ab}}. \tag{4}$$

In section 3, we will discuss the experimental complexities in dual-colour FCS such as spectral cross-talk, imperfect overlap of the detection volumes or incomplete labelling of the binding partners and show how to avoid them or take them into account during data analysis (see also table 1).

2.3. Dual-focus cross-correlation

Dual-focus FCS overcomes the problem of determining the size of the detection area w, which is necessary for quantitative analysis of FCS correlation curves. w cannot be inferred by fitting auto-correlation curves since it is always coupled to the diffusion coefficient in the form of the diffusion time $\tau_D = w^2/4D$ (2). Usually, it is determined by a calibration measurement using a free dye in solution with a known diffusion coefficient. Optical distortions or saturation leads to a change in the size of the detection area, rendering quantitative measurements challenging. Dual-focus FCS employs two spatial detection areas in a well-defined lateral distance d [9]. From the two intensity traces $F_1(t)$ and $F_2(t)$ the two auto-correlation curves (1) and also the spatial cross-correlation curves $\tilde{G}^{12}(\tau)$ and $\tilde{G}^{21}(\tau)$ can be calculated (figure 1(d)):

$$\tilde{G}^{12}(\tau) = \frac{\langle \delta F_1(t) \delta F_2(t+\tau) \rangle}{\langle F_1(t) \rangle \langle F_2(t) \rangle} = \frac{\tilde{g}^{12}(\tau)}{\langle F_1(t) \rangle \langle F_2(t) \rangle}. \tag{5}$$

This spatial cross-correlation function depends on w and D independently, which can both be determined from the fit. Hence, a calibration measurement to determine w is dispensable. The symmetry relation $\tilde{G}^{12}(\tau) = \tilde{G}^{21}(\tau)$ is only valid in the absence of directed motion of the particles.

Note that in practice an alternating excitation of the two detection volumes is necessary for the separation of the signal from the two overlapping measurement volumes.

2.4. Dual-focus dual-colour cross-correlation

A calibration of the size of both the red and the green detection volume, w_r and w_g, and their axial displacement due to chromatic aberrations d_{rg} can be avoided by simultaneous dual-focus dual-colour FCS (figure 1(e)). As in dual-focus FCS, two detection volumes at two spatial positions (distance d) are used. In each position, both the red and the green intensity are recorded. This results in four different intensity signals $F_{r1}(t)$, $F_{r2}(t)$, $F_{g1}(t)$ and $F_{g2}(t)$, from which 16 correlation curves can be calculated. In the case of free diffusion, the absence of directed motion, and the same geometries at both positions, only 6 of these 16 correlation curves are distinct (figure 1(f)) and can be described by the model functions shown in table 3 (derivation in appendix A). The global fit of all experimental correlation curves can be used to determine all physical parameters of interest (table 2). However, in non-ideal systems it

Table 3. Correlation functions taking into account spectral cross-talk and triplet.

Non-normalized correlation functions from single-species correlation functions (table 2(b)):

$$\begin{aligned} g_{\mathrm{rr}} &= g_{\mathrm{rr}}^{\mathrm{a}} + g_{\mathrm{rr}}^{\mathrm{ab}} + \kappa^2 g_{\mathrm{gg}}^{\mathrm{b}} + \kappa^2 g_{\mathrm{gg}}^{\mathrm{ab}} + 2\kappa g_{\mathrm{rg}}^{\mathrm{ab}}, \\ g_{\mathrm{rg}} &= g_{\mathrm{rg}}^{\mathrm{ab}} + \kappa g_{\mathrm{gg}}^{\mathrm{b}} + \kappa g_{\mathrm{gg}}^{\mathrm{ab}}, \\ g_{\mathrm{gg}} &= g_{\mathrm{gg}}^{\mathrm{b}} + g_{\mathrm{gg}}^{\mathrm{ab}}, \end{aligned} \tag{6}$$

where κ is the cross-talk coefficient (15).

Normalized correlation functions:

$$G_{\mathrm{rg}} = \frac{g_{\mathrm{rg}}}{F_{\mathrm{r}} F_{\mathrm{g}}}, \tag{7}$$

Intensities:

$$\begin{aligned} F_{\mathrm{r}} &= \eta_{\mathrm{r}}(C_{\mathrm{a}} + C_{\mathrm{ab}}) + \kappa \eta_{\mathrm{g}}(C_{\mathrm{b}} + C_{\mathrm{ab}}), \\ F_{\mathrm{g}} &= \eta_{\mathrm{r}}(C_{\mathrm{b}} + C_{\mathrm{ab}}). \end{aligned} \tag{8}$$

Channel brightness used for fitting:

$$\eta_{\mathrm{r}} = \frac{F_{\mathrm{r}}^m - \kappa F_{\mathrm{g}}^m}{C_{\mathrm{a}} + C_{\mathrm{ab}}}, \quad \eta_{\mathrm{g}} = \frac{F_{\mathrm{g}}^m}{C_{\mathrm{b}} + C_{\mathrm{ab}}}. \tag{9}$$

Single-species correlation functions for Gaussian detection volumes:

$$\text{3D:} \quad g_{\mathrm{rg}}^i = \eta_{\mathrm{r}} \eta_{\mathrm{g}} C_i \left(\frac{2}{\pi}\right)^{3/2} \gamma_x^2 \gamma_z \exp\left[-2d_{\mathrm{rg}}^2 \gamma_z^2 - 2d^2 \gamma_x^2\right], \tag{10}$$

$$\begin{aligned} &\text{2D:} \quad g_{\mathrm{rg}}^i = \eta_{\mathrm{r}} \eta_{\mathrm{g}} C_i \tfrac{2}{\pi} \gamma_x \gamma_z \exp\left[-2d_{\mathrm{rg}}^2 \gamma_z^2 - 2d^2 \gamma_x^2\right], \\ &\text{with:} \quad \gamma_x = \left(8D_i\tau + w_{\mathrm{r}}^2 + w_{\mathrm{g}}^2\right)^{-1/2}, \quad \gamma_z = \left(8D_i\tau + w_{\mathrm{r}}^2 S_{\mathrm{r}}^2 + w_{\mathrm{g}}^2 S_{\mathrm{g}}^2\right)^{-1/2}, \end{aligned} \tag{11}$$

$i = \{\mathrm{a}, \mathrm{b}, \mathrm{ab}\}$. Single colour: r $\rightarrow$ g or g $\rightarrow$ r and $d_{\mathrm{rg}} = 0$. Single-focus: $d = 0$. With these expressions correlation functions describing all six experimental correlation curves (single/dual-focus, single/dual-colour, table 2(a)) can be calculated.

Blinking and triplet:

$$\begin{aligned} &g_{\mathrm{rr}}^i \rightarrow (1 + T_i(\tau)) g_{\mathrm{rr}}^i; \quad g_{\mathrm{gg}}^i \rightarrow (1 + T_i(\tau)) g_{\mathrm{gg}}^i; \quad g_{\mathrm{rg}}^i \rightarrow g_{\mathrm{rg}}^i, \\ &T_i(\tau) = \tfrac{f_{\mathrm{T}}^i}{1 - f_{\mathrm{T}}^i} \mathrm{e}^{-\tau/\tau_{\mathrm{T}}^i} \end{aligned} \tag{12}$$

For definitions of the parameters see table 2.

might be necessary to reduce the number of free fitting parameters by additional assumptions or calibration measurements (see section 4.3).

Here, we assume that the corresponding green and red foci are laterally centred onto each other, with a possible shift only in the axial direction. For certain realizations of dual-colour dual-focus FCS there can, however, be a lateral displacement between red and green foci, resulting in different lateral distance d between the two green and the two red foci ($d_{\mathrm{r}} \neq d_{\mathrm{g}}$). This can be taken into account in (10) and (11) and also in dual-colour single-focus correlation measurements.

3. Factors affecting the measurement

3.1. Size of detection volumes, imperfect overlap

A complication in dual-colour FCS is that usually the red and the green detection volume have different sizes and that chromatic aberrations cause an axial shift between the detection volumes. The resulting imperfect overlap leads to a reduced cross-correlation [18]. Quantitative analysis of spectral cross-correlation curves requires the knowledge of the spatial overlap, as well as the sizes of the red and the green detection volume, w_g and w_r. Due to optical (triplet) saturation, w_r and w_g depend on the excitation intensity and the fluorophore used. They can be determined by a calibration measurement using dyes with a known diffusion coefficient. Calibration of the overlap between the detection volumes is more difficult and requires a cross-correlation standard with a known degree of double labelling. Often short DNA or RNA labelled with both a red and a green fluorophore is used, but 100% labelling can not usually be guaranteed. Since a change of the fluorophores or of the excitation intensity results in different saturation, all calibration measurements have to be performed under conditions identical to the later experiment.

The calibration of the detection volumes and their overlap can be circumvented if, in addition to two spectral channels, also two spatial channels are employed (see section 2.4). Then w_r, w_g and d_{rg} are free fitting parameters and the distance d between the foci is calibrated instead. This is much easier and, most importantly, hardly influenced by the sample.

3.2. Fluorescent background

A common source for a fluorescent background is auto-fluorescence, but also detector dark counts, ambient light, incompletely blocked laser light or water Raman scattering can lead to a significant change of the correlation amplitudes, especially for low fluorophore concentrations. A mean background B_r and B_g in the red and green channels, respectively, reduces the amplitude of the cross-correlation curve [19]:

$$\tilde{G}_{rg}^{meas} = \tilde{G}_{rg}^{true} \frac{F_r^m}{F_r^m + B_r} \frac{F_g^m}{F_g^m + B_g} \tag{13}$$

where $F_r^m = \langle F_r \rangle - B_r$ and $F_g^m = \langle F_g \rangle - B_g$ are the mean fluorescence intensities excluding the background, and $\langle F_r \rangle$ and $\langle F_g \rangle$ are the measured mean intensities including the background. The expressions for the auto-correlation curves can be obtained by setting $g = r$.

The average background intensities B_r and B_g need to be measured in a sample containing no fluorescent molecules. In cellular measurements, auto-fluorescence levels can change from measurement to measurement, rendering accurate background measurements difficult. A solution is to monitor fluorescence far away from the emission from the fluorescent molecules in a third spectral channel [19]: B_r and B_g can be related to intensities measured in an ultraviolet (UV) or far-red channel by calibration measurements without fluorescent molecules. During the actual experiment, the background intensities are then calculated from the intensity in the third channel. However, this approach relies on a fixed spectral profile of the background.

One possibility to take into account the background is to include the background related factor (12) in the model functions used for data fitting. Another option is to correct the measured correlation curves prior to fitting:

$$\tilde{G}_{rg}^{true} = \tilde{G}_{rg}^{meas} \frac{\langle F_r \rangle}{\langle F_r \rangle - B_r} \frac{\langle F_g \rangle}{\langle F_g \rangle - B_g}. \tag{14}$$

If the fluorescent background is not constant during the measurement time but is decaying due to photobleaching, the resulting correlation curves are seriously distorted and intensity signals have to be corrected prior to calculating the correlation curves (section 3.7).

3.3. Spectral cross-talk

A major problem in dual-colour FCS is spectral cross-talk, usually from the green fluorophore into the red channel. This introduces additional similarities between the fluorescence fluctuations in the two channels and can therefore result in a false-positive cross-correlation [18]. An elegant way to avoid spectral cross-talk is the use of alternating excitation [20, 21]. Here the fluorophores are excited alternatingly only with one laser and fluorescence is collected only in one channel. In this way, signals from different species can be separated completely. The repetition rate needs to be faster than the timescale of interest, since the minimum time resolution is determined by the switching time.

Alternating excitation is usually not implemented in standard FCS instruments. Although it is preferable to avoid spectral cross-talk during data acquisition, it is also possible to take it into account during the fitting of the correlation curves [22] (see table 3, appendix B). This requires the knowledge of the cross-talk coefficient κ, which depends only on the green fluorophore, the green excitation intensity and the optical setup. It can be easily measured using a green-only sample as

$$\kappa = \frac{F_{\mathrm{r}}^{\mathrm{m}}}{F_{\mathrm{g}}^{\mathrm{m}}}, \tag{15}$$

where $F_{\mathrm{r}}^{\mathrm{m}}$ and $F_{\mathrm{g}}^{\mathrm{m}}$ are the background-corrected average intensities (see section 3.2).

3.4. Incomplete and stochastic labelling

In actual experiments, usually not all molecules of interest carry a fluorescent label. The use of fluorescent proteins fused to the target proteins seems to guarantee complete labelling. However, in practice, incomplete maturation or misfolding also results in incomplete labelling. In the case of external labelling with organic dyes, not all binding sites will eventually carry a fluorophore. A related scenario is stochastic labelling: if the dye can bind to more than one site, this results in multiple labels on one molecule. The same is the case if several fluorescent proteins are fused to the protein of interest in the form of a tandem multimer to increase the brightness. The different brightnesses of the individual molecules have to be considered during data fitting to avoid serious errors in the obtained concentrations.

Incomplete labelling or multiple labelling can be taken into account with the same mathematical formalism (table 5). A molecule a carries K red fluorophores with a probability distribution $p(K)$. The average number of fluorophores on one molecule is $\bar{K}$. A molecule b carries L fluorophores with a probability $p(L)$. Usually it is possible to make an assumption about the number of binding sites. Then, the second moments $\overline{K^2}$ and $\overline{L^2}$ of the corresponding distributions, which are needed for data fitting, can be calculated from $\bar{K}$ and $\bar{L}$ if the type of the distribution is known (see table 4).

On purified samples, $\bar{K}$ and $\bar{L}$ can be measured accurately by absorption spectroscopy. Here the absorption in the UV, originating from the proteins, is compared with the absorption at the absorption wavelength of the fluorophore. In cellular systems with fluorescent proteins, a fusion of both the red and the green protein to the protein of interest (or a similar protein) can be used to determine the maximum amount of cross-correlation and hence the labelling efficiency.

Table 4. Distributions for stochastic labelling. $\bar{K}$ is the mean number of fluorophores on a molecule.

Distribution	Second moment	Application
Bernoulli	$\overline{K^2} = \bar{K}$	Incomplete labelling
Binomial	$\overline{K^2} = \bar{K}\left(1 + \bar{K} - \bar{K}/N\right)$	A defined number of binding sites N
Poisson	$\overline{K^2} = \bar{K} + \bar{K}^2$	A large number of binding sites N, $\bar{K} \ll N$

Also the presence of endogenous, unlabelled proteins leads to effectively incomplete labelling. If the labelling efficiency of the labelled proteins and their degree of binding are known, this allows one to extract the concentrations of the endogenous binding partners [6, 19].

3.5. Multiple binding sites

If a molecule has multiple binding sites and can aggregate, the complex will carry A molecules of species a and B molecules of species b. Usually, the numbers A and B vary from complex to complex and are described by the probability distribution $p(A, B)$. Similar to the case of stochastical labelling, the parameters for characterizing the probability distribution $p(A, B)$ are the first and second moments $\bar{A}$, $\bar{B}$, $\overline{AB}$, $\overline{A^2}$ and $\overline{B^2}$ (C.11)–(C.13). These parameters should be determined by assumptions about the binding process. If there is additional information available about the system, it might be possible to extract some of these parameters by data fitting.

The fitting functions for multiple binding sites can be found in table 5. Note that oligomerization of a single species a is also described by this formalism, which makes it useful also for single-colour auto-correlation measurements [23].

3.6. Blinking and triplet dynamics

Most fluorescent molecules show fast photophysical intensity fluctuations. One source is the population of the metastable triplet state. On timescales shorter than the lifetime of this state, the number of bright molecules in the sample is reduced. The fraction of dark molecules and the timescale depend on the excitation intensity. Another source is internal dynamics e.g. due to protonation–deprotonation dynamics. This blinking is rather strong for fluorescent proteins. It depends on the pH of the solution, but hardly on the laser excitation intensity.

Blinking can be incorporated into the model function by an exponential decay term ((12), [7]). Blinking between two distinct fluorophores is not correlated. Therefore, cross-correlation terms are not affected. In the case of multiple labels on a single molecule or binding of multiple molecules in a single complex, the dark fraction is reduced, since blinking of labels on a single molecule is not correlated. In this case, blinking can be incorporated into the model functions by a rather simple substitution ((19), derivation in appendix D).

If the blinking timescale is comparable to the diffusion time, it is difficult to distinguish these processes during data fitting. A calibration of the blinking time and fraction is recommended using a viscous sample to increase the diffusion time to values much larger than the blinking time. Care must be taken that the blinking is not affected by the new environment (e.g. the same pH value as in the actual measurement). In dual-focus measurements, blinking

Table 5. Incomplete and multiple labelling and multiple binding sites.

Non-normalized correlation functions:

$$g_{rr} = \overline{K^2} g_{rr}^{a} + \kappa^2 \overline{L^2} g_{gg}^{b} + (\bar{A}\overline{K^2} + (\overline{A^2} - \bar{A})\bar{K}^2) g_{rr}^{ab} + \kappa^2 (\bar{B}\,\overline{L^2} + (\overline{B^2} - \bar{B})\bar{L}^2) g_{gg}^{ab} + 2\kappa\,\overline{AB}\,\bar{K}\bar{L} g_{rg}^{ab},$$

$$g_{rg} = \overline{AB}\,\bar{K}\bar{L} g_{rg}^{ab} + \kappa(\bar{B}\,\overline{L^2} + (\overline{B^2} - \bar{B})\bar{L}^2) g_{gg}^{ab} + \kappa\,\overline{L^2}\, g_{gg}^{b}, \tag{16}$$

$$g_{gg} = \overline{L^2}\, g_{gg}^{b} + (\bar{B}\,\overline{L^2} + (\overline{B^2} - \bar{B})\bar{L}^2) g_{gg}^{ab},$$

where $\bar{K}$ ($\bar{L}$) is the mean number of red (green) fluorophores on molecule A (B). $\overline{K^2}$ and $\overline{L^2}$ are the second moment of the labelling distribution and can be estimated from $\bar{K}$ and $\bar{L}$ (table 4). $\bar{A}$, $\bar{B}$, $\overline{A^2}$, $\overline{B^2}$ and $\overline{AB}$ characterize the stoichiometry of the complex and are defined in (C.11)-(C.13).

Intensities:

$$\begin{aligned} F_g &= \eta_g \bar{L}(C_b + \bar{B}C_{ab}), \\ F_r &= \eta_r \bar{K}(C_a + \bar{A}C_{ab}) + \eta_g \kappa \bar{L}(C_b + \bar{B}C_{ab}). \end{aligned} \tag{17}$$

Channel brightness used for fitting:

$$\eta_r = \frac{F_r - \kappa F_g}{\bar{K}(C_a + \bar{A}C_{ab})}, \quad \eta_g = \frac{F_g}{\bar{L}(C_b + \bar{B}C_{ab})}. \tag{18}$$

Blinking and triplet:

$$\overline{K^2} \to \overline{K^2}(\tau) = \overline{K^2} + \bar{K}T_a(\tau), \quad \overline{L^2} \to \overline{L^2}(\tau) = \overline{L^2} + \bar{L}T_b(\tau), \quad T_a(\tau) = \frac{f_T^a}{1 - f_T^a} e^{-\tau/\tau_T^a}. \tag{19}$$

1 : 1 binding stoichiometry:

$$\bar{A} = \overline{A^2} = \bar{B} = \overline{B^2} = \overline{AB} = 1. \tag{20}$$

and diffusion can be readily distinguished due to their different effects on the cross-correlation curve.

Note that the intensity dependence of triplet blinking results in different blinking behaviours at different positions in the detection area. Equation (12) is a commonly used approximation, where f_T and τ_T are effective triplet fraction and triplet time.

3.7. Depletion due to photobleaching, bleaching of a background, external instabilities

FCS measurements require a stationary state. Otherwise, slow changes of the intensity during the measurement time lead to strong distortions of the correlation curves (figure 2(a)). In particular, in *in vivo* measurements, this condition is not always fulfilled. If the reservoir of fluorophores is limited, even weak photobleaching leads to a reduction of the fluorescent molecules with time. This artefact is strongest for high concentrations, since here the changes in the intensity due to depletion can be much larger than the fluctuations due to diffusion through the detection area. Another reason for a decaying average intensity in cellular systems is the bleaching of the auto-fluorescent background or of immobilized fluorophores. If very high concentrations are used, also external instabilities (e.g. fluctuations of the laser power) can result in fluorescence fluctuations with amplitudes comparable to those caused by diffusion.

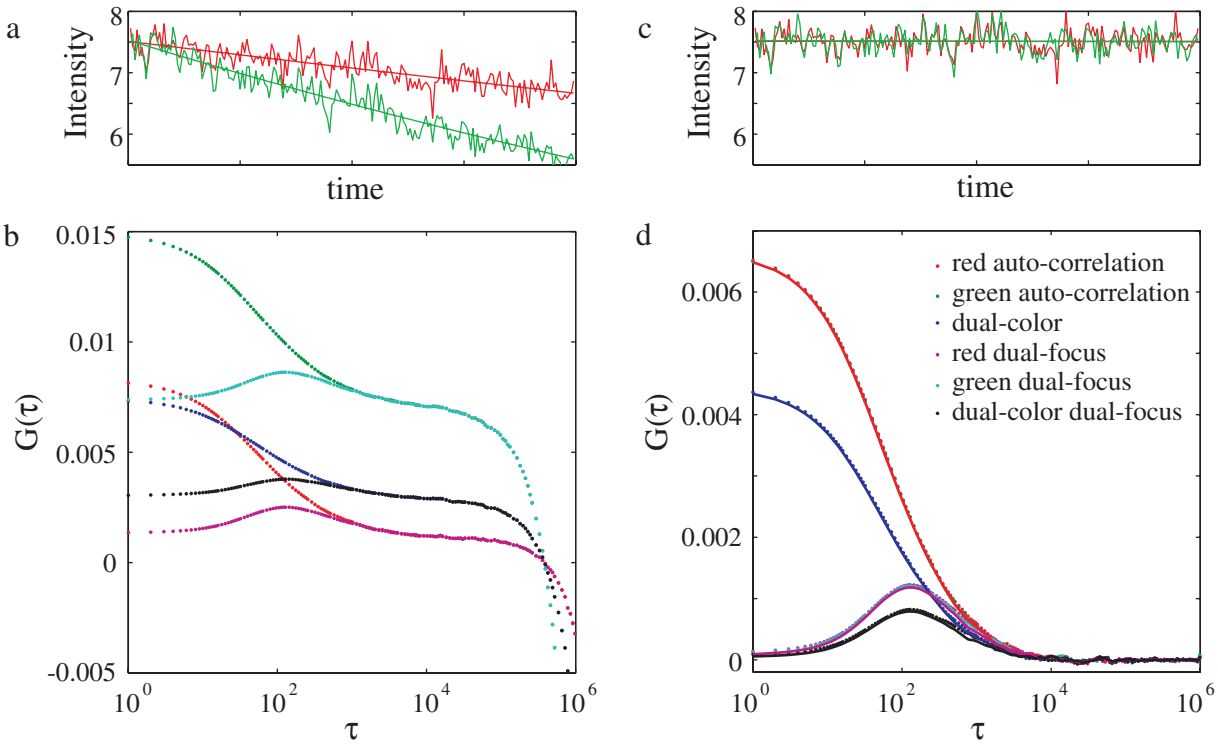

Figure 2. Correction for depletion due to photobleaching. (a) Simulated intensities and (b) resulting correlation curves with depletion due to photobleaching. The decay of the intensities leads to strong distortions of the correlation curves. (c) Corrected intensity traces. (d) Correlation curves calculated based on corrected intensities (·) and simulations without depletion due to photobleaching (—). Parameters for the 2D simulation: $D_r = D_g = D_{rg} = 400\,\mu m^2\,s^{-1}$, $w_r = w_g = 0.2\,\mu m$, $S_r = S_g = 4$, $C_r = C_g = 50\,\mu m^{-2}$, $C_{rg} = 100\,\mu m^{-2}$, $d = 0.2\,\mu m$ and $d_{rg} = 0$. Constant bleaching probabilities in the simulation box (size $8 \times 8\,\mu m^2$): $p_r = 0.2\,s^{-1}$, $p_g = 0.5\,s^{-1}$. For details of the simulation see [25].

A common way of reducing this artefact is to evaluate only short time intervals, during which the intensity change is small and to average the resulting correlation curves. However, the choice of too short traces (duration $T_m < 10^5 \tau_D$) leads to systematic distortions of the curves [24] and the artefact is only partially reduced. Fortunately, there is a way to correct for a slow change in the average intensity completely if the source of these changes can be identified [25]. The first step is to approximate the measured intensities $F_r(t)$ and $F_g(t)$ by analytical functions $f_r(t)$ and $f_g(t)$. Then the intensities are transformed using these functions to result in corrected intensities which are indistinguishable from a steady state. Correlation curves calculated based on these corrected intensities are free of distortions. In the following, we discuss the correction for the three different cases mentioned above. If the source of the intensity changes cannot be attributed to one of the cases alone, the correction still leads to apparently undistorted curves, but the amplitudes and therefore the measured concentrations might be incorrect.

3.7.1. Depletion of fluorophores. For a restricted reservoir and low bleaching rates [26], the decay can be approximated by an exponential and for the analytical functions we can choose: $f(t) = f_0 e^{-t/t_b}$. In general, a multi-exponential decay results in a better approximation of the decaying intensity; often two exponentials are sufficient. With the knowledge of $f(t)$ the intensities can be corrected prior to calculating the correlation curves in the following way:

$$F^c(t) = \frac{F(t)}{\sqrt{f(t)/f_0}} + f_0\left(1 - \sqrt{f(t)/f_0}\right). \tag{21}$$

This transformation leads to a constant mean value and constant fluctuations with time, not distinguishable from a system in a steady state. The correlation curve calculated from the corrected intensity $F^c(t)$ is no longer distorted by the decaying intensity and the concentration inferred by fitting is the initial concentration (figure 2(b)). Note that, in general, $F_r(t)$ and $F_g(t)$ have to be corrected using different functions $f_r(t)$ and $f_g(t)$. Also, this approach does not correct for the apparent reduction of the concentration and diffusion time due to bleaching in the detection volume (compare section 3.9).

Photobleaching leads to a reduction in the double-labelled molecules and consequently to a reduction of the cross-correlation amplitude. Therefore, cross-correlation curves calculated with the corrected intensity F_r^c, F_g^c have too low amplitudes. But multiplication of the cross-correlation curves by a simple factor

$$f_D = \left(\frac{\langle F_r^c(t)\rangle\langle {}^cF_g(t)\rangle}{\langle F_r(t)\rangle\langle F_g(t)\rangle}\right)^{1/2} \tag{22}$$

results in cross-correlation curves indistinguishable from the case where no depletion due to photobleaching is present (figure 2(b)).

This correction is valid only if molecules carry maximally one fluorophore; otherwise it will lead to the overestimation of amplitudes.

3.7.2. Bleaching of the fluorescent background. Bleaching of an auto-fluorescent background or of immobilized fluorophores can be approximated by a (multi-)exponential decay with an offset f_0, corresponding to the average intensity of the mobile fluorophores to be measured: $f(t) = \sum_k f_k \exp(-t/t_{b,k}) + f_0$. To correct for this artefact, the intensity originating from the decaying background is subtracted from the measured intensity $F(t)$ before correlation:

$$F_c(t) = F(t) - (f(t) - f_0). \tag{23}$$

3.7.3. Changes in excitation intensity. The analytical function $f(t)$ to describe a varying intensity is usually rather complex, involving e.g. polynomials or trigonometric functions. To correct for this artefact, the intensity is simply rescaled:

$$F_c(t) = F(t)\frac{f(0)}{f(t)}. \tag{24}$$

3.8. Membrane movements

Binding studies on membranes using dual-colour FCS are especially challenging due to several reasons [27]: the slow diffusion leads to strong photobleaching and long measurement times, the detection volume has to be positioned on the membrane with a high accuracy to avoid an enlargement of the detection area due to the divergence of the laser beam and the membrane has to be stable with respect to the detection volume to avoid distortions of the correlation curves. Membrane movements also lead to a false positive cross-correlation, since they cause correlated fluctuations of the two labelled molecules even in the absence of co-diffusion.

These problems can be circumvented employing scanning FCS [10], where the detection volume is repeatedly scanned through a vertical membrane perpendicularly (see section 5.1).

3.9. Photobleaching

Whereas depletion due to photobleaching can be easily corrected for, the direct effect of photobleaching on the correlation curves remains: photobleaching of fluorophores in the detection volume leads to reduced residence times and therefore to apparently faster diffusion. In addition, the concentration of bright fluorophores is reduced at the centre of the detection volume ('hole burning'), leading to complex effective detection volumes, which cannot be described well by model functions [28]. The system can still reach a steady state, the number of bleached molecules is equal to molecules diffusing into the detection volume, and the average intensity is constant. Therefore, photobleaching cannot be identified by examining the temporal dependence of the intensity. Additionally, in the case of a not extremely strong photobleaching the shape of the correlation curves is not necessarily changed. To identify photobleaching, it is therefore usually necessary to measure in the same system with different excitation intensities to identify the maximum excitation intensity where the fitting parameters are not yet affected. Note that this maximum intensity scales proportionally with the diffusion coefficient.

In dual-focus FCS photobleaching becomes more apparent, since it changes the relative amplitudes of auto- and spatial cross-correlation curves. Fitting such curves results in unphysically small apparent detection volumes.

3.10. Quenching and Förster resonance energy transfer (FRET)

Due to FRET or quenching, the brightness of the fluorophores in the complex (η_r^{ab}, η_g^{ab}) can be different from that in the monomeric molecules (η_r, η_g). With the definitions

$$q_r = \frac{\eta_r^{ab}}{\eta_r}, \quad q_g = \frac{\eta_g^{ab}}{\eta_g}, \tag{25}$$

the change in brightness can be taken into account in (6):

$$\begin{aligned} g_{rr}^{ab} &\to q_r^2 g_{rr}^{ab}, \\ g_{gg}^{ab} &\to q_g^2 g_{gg}^{ab}, \\ g_{rg}^{ab} &\to q_r q_g g_{rg}^{ab}. \end{aligned} \tag{26}$$

In practice, however, calibration of q_r and q_g might be difficult. Since the changes in the brightnesses of a carefully chosen fluorophore pair are typically small, neglecting them usually leads to only moderate errors.

3.11. Anomalous diffusion, multi-component diffusion

In many cellular experiments, the correlation curves are not well described by a single-component model. Crowding or transient interactions lead to apparent anomalous diffusion, and binding to larger complexes results in multi-component diffusion. Correlation functions for anomalous diffusion can be obtained by replacing τ by τ^α in (10) or (11). The D_i are then the anomalous transport coefficients [7, 29].

For multi-component diffusion every component is treated as an individual species. The single-species correlation functions (equation (10) or (11)) are summed up:

$$g_{\mathrm{rg}}^{i} \rightarrow \sum_{k} g_{\mathrm{rg}}^{i,k}. \tag{27}$$

Note that the use of multi-component correlation functions increases the number of fitting parameters, rendering accurate parameter estimates more difficult.

3.12. Detector artefacts

After registering a photon, single-photon detectors are not able to register a second photon within the dead time ($\approx$100 ns). Correlations at times below the dead time cannot be resolved. For high count rates, the dead time effect distorts the correlation curve at small timescales. In addition, the electronic saturation has an effect very similar to optical saturation, resulting in an enlarged detection volume [30].

It sometimes happens that shortly after a photon event, a second event is reported without a photon actually incident on the detector. These two signals are highly correlated and lead to a peak in the auto-correlation curves for small lag times. This afterpulsing peak can mask the triplet contributions and even influence the measured diffusion times. An elegant way to avoid the afterpulsing artefact is to split the emission behind the pinhole with a beam splitter and to detect the signal with two detectors. The cross-correlation curve now lacks the afterpulsing artefact, since afterpulsing events are not correlated between the detectors.

If the arrangement with two detectors cannot be used, it is possible to correct the correlation curves for the afterpulsing artefact [31]. To this end, calibration correlation curves $\tilde{G}_{\mathrm{AP}}(\tau)$ with a constant light source are obtained for individual avalanche photo diodes (APD). Measured correlation curves $\tilde{G}^m(\tau)$ can then be corrected:

$$\tilde{G}^c(\tau) = \tilde{G}^m(\tau) - \bar{G}_{\mathrm{AP}}(\tau)\frac{F_{\mathrm{AP}}}{\langle F\rangle}, \tag{28}$$

where F_{AP} is the average count rate with which the calibration curve $\tilde{G}_{\mathrm{AP}}(\tau)$ has been obtained, and $\langle F\rangle$ is the average count rate during the experiment. Good results can be attained if the afterpulsing calibration curve is smoothed by approximating it on a double logarithmic scale with an analytical function, i.e. a polynomial $\bar{G}_{\mathrm{AP}}(\tau)$.

3.13. Single bright events and irregular curves

Singular bright events, resulting from aggregates or bright vesicles and recognizable in the intensity trace as spikes, can dominate the entire correlation curve [3]. But also photobleaching of the auto-fluorescent background or of immobilized molecules, depletion due to photobleaching or a change in the local environment due to sample movements may lead

to slow changes in the fluorescence signal and distorted correlation curves [32]. The most common ways to reduce the impact of the above-mentioned imperfections are [3] (i) to take several short measurements instead of one long measurement, (ii) to manually discard distorted correlation curves and (iii) to fit the average of the remaining curves with a model function describing one additional mobile species. This additional component in the correlation function, sometimes combined with an overall offset, approximates the distorted part of the experimental correlation curve at larger lag times. This approach is not optimal. Hand-selection of curves is time-consuming and is often ambiguous with the danger of introducing a subjective bias. In addition, the distorted parts of the correlation curve can often not be described well by only one additional component leading to a strong error and bias in the parameters of interest and the introduced additional free fitting parameters can render the fit results ambiguous. Methods for automated rejection of corrupted parts of the data are currently being developed and these will be very useful once incorporated into standard FCS analysis software [32].

4. Data analysis

A complete FCS measurement consists of several steps (see table 6): calibration measurements to determine as many parameters as possible, the actual data acquisition, correction of correlation curves for background or depletion due to photobleaching, and finally the fitting of the data to extract the parameters of interest. In this section we concentrate on the last point, the fitting of the data with model functions, taking into account all relevant experimental complexities. The steps involved in calculating the model function are also listed in table 6.

4.1. Fitting of auto- and cross-correlation curves

The calculated and corrected correlation curves are fitted to the model using standard fitting procedures as implemented in common data analysis software (Matlab, Origin, etc). The results of the fit are the optimal parameter values that minimize the difference between the model and the data (residuals). In contrast to auto-correlation measurements, dual-colour dual-focus measurements require simultaneous (global) fitting of all 16 acquired correlation curves. Here, the sum of all squared residuals is minimized.

We recommend the use of weighing of the data points to achieve fits unbiased towards the noisier data points. The weights of a data point can be estimated by comparing the variations between data points in its vicinity or by computing the variation of data points between consecutive measurements.

4.2. Global analysis of several measurements

In repeated measurements some parameters can vary from measurement to measurement (C_a, C_b, C_{ab}), whereas others are most likely the same (e.g. geometrical parameters w_r, w_g, w_{rg}, d_{rg}). Linking those parameters during a global analysis of several sets of measurements can greatly increase the accuracy of the parameter estimates [33].

4.3. Reduction of free fitting parameters

If too many free fitting parameters are employed, their values become unreliable even in the case of a perfect fit. Measurements become more reliable if as many parameters as possible are

Table 6. Steps involved in FCCS.

(i) Determination of parameters by calibration measurements:

- (a) Measure background levels B_r, B_g in the sample without fluorophores.
- (b) Determine cross-talk coefficient κ in a green-only sample.
- (c) Incomplete or statistical labelling: measure $\bar{K}$, $\bar{L}$. Calculate $\overline{K^2}$ and $\overline{L^2}$ (table 4).
- (d) Single-focus measurements: calibrate w_r, w_g, overlap d_{rg}.
- (e) If possible, determine f_T, τ_T, S_r, S_g, ... (section 4.3).

(ii) Experiment: acquire correlation curves and average intensities (table 2(a)).

(iii) If required: correct intensities for depletion due to photobleaching, external instabilities or bleaching of the background (section 4.2). Calculate correlation curves based on corrected intensities.

(iv) Correct measured correlation curves for fluorescent background with (14).

(v) Fit auto and cross-correlation curves using a nonlinear least-squares fit (see section 4).

The fitting function has as input parameters the free fitting parameters, the fixed additional parameters and the experimental mean intensities F_r^m, F_g^m (table 2). It evaluates the following steps:

(i) Calculate the channel brightness parameters η_r and η_g ((9) and (18)).

(ii) Calculate single-species correlation functions ((10) and (11)).

(iii) Incorporate the blinking term:

- (a) maximally one label: (12).
- (b) multiple labelling or multiple binding sites: calculate $\overline{K^2}(\tau)$, $\overline{L^2}(\tau)$ (19).

(iv) Calculate non-normalized correlation functions ((6) or (16)).

(v) Calculate normalized correlation functions (7).

determined previously by a calibration measurement and kept fixed during the data fitting. This is especially important in *in vivo* measurements where the curves are usually of only moderate quality. In the following, we discuss how to reduce the number of free fitting parameters:

4.3.1. Size of the detection volumes w_r, w_g and spatial overlap of detection volumes. For single-focus measurements the parameters describing the size of the detection volumes and their overlap need to be determined by a calibration measurement. Since optical artefacts and saturation change these parameters, a calibration measurement needs to be performed under conditions identical to the later measurement using the same dye. The spatial overlap can be estimated using a cross-correlation standard. Note that in practice a cross-correlation standard usually does not show 100% cross-correlation. For dual-focus measurements, a prior calibration of w_r, w_g or d_{rg} is not necessary. However, since these parameters do not vary from measurement to measurement, the accuracy can be significantly enhanced by linking these parameters during a global analysis of a set of data from several measurements.

4.3.2. Structure parameters S_r, S_g. The structure parameter (aspect ratio of the detection volume $S = w_z/w_{x,y}$) is a delicate parameter. If measurement conditions are not optimal, this parameter often accounts for other distortions of the correlation curves and assumes too large values. This directly affects the estimates of the concentrations. Calibration of S_r and S_g or linking during global analysis is often necessary. If this is not possible, fixation of these parameters to a standard value (e.g. 4.5 or 5 [5]) often results in smaller errors than allowing them to assume unphysical values during the fit.

4.3.3. Blinking and triplet parameters f_T, τ_T. Triplet or blinking parameters can also be linked during the global analysis or determined with a calibration measurement. In the case of fast diffusion, it is difficult to distinguish the blinking from the diffusional part of the curve. In this case, the choice of a more viscous medium will improve the calibration measurement. Since blinking is pH dependent, the calibration buffer has to be adapted to the later experiment. Note that the afterpulsing artefact is not easily distinguished from the triplet. In case it cannot be avoided by using two detectors, it should be corrected for as described above if fast timescales are required.

4.3.4. Channel brightness η_r, η_g. The channel brightness values η_r and η_g can be calibrated in a simple system consisting of monomeric fluorophores in a background-free medium. Care must be taken that the excitation intensity and chemical properties of the calibration solution (e.g. pH) are identical to the later measurement and that distortions of the detection volume remain minimal.

If the channel brightness has been calibrated, in simple systems the background can be treated as a free fitting parameter. In particular, in cellular systems, where background values can vary from measurement to measurement, this might be a valuable alternative.

4.3.5. Degrees of labelling $\bar{K}$, $\bar{L}$. The average number of fluorophores on a molecule ($\bar{K}$, $\bar{L}$) can be determined by absorption spectroscopy by comparing the magnitude of the protein absorption band in the UV with the absorption at the fluorophore absorption maximum. Second moments $\overline{K^2}$, $\overline{L^2}$ can be calculated from $\bar{K}$, $\bar{L}$ if an assumption about the number of binding sites on one molecule can be made (see table 4).

4.3.6. Diffusion coefficients D_a, D_b, D_{ab}. Assumptions about the molecular weight of the molecules allow us to estimate their diffusion coefficients. In the case of 1 : 1 binding without any additional factors, one free fitting parameter D_a is sufficient to take into account the viscosity of the surrounding. D_b and D_{ab} can be related to D_a via their molecular weights:

$$D_b = D_a\,(m_b/m_a)^{1/3}\,, \qquad D_{ab} = D_a\,((m_a + m_b)/m_a)^{1/3}\,. \tag{29}$$

In membranes, the dependence of the diffusion coefficient on the size of the diffusing molecule is weaker than in free solution. For larger entities it follows the logarithmical Saffman–Delbrueck equation. In this case either all diffusion coefficients can be assumed approximately equal ($D_a = D_b = D_{ab}$) or $D_{ab} = \min(D_a, D_b)$.

In homogenous samples, global linking of diffusion coefficients during a global analysis is another alternative.

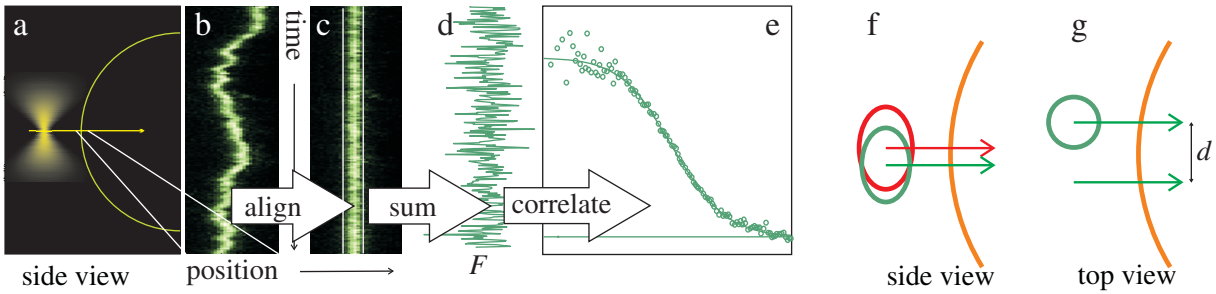

Figure 3. Principle of scanning FCS. (a) In scanning FCS, the detection volume is repeatedly scanned perpendicularly through a vertical membrane. The individual line scans can be arranged as a pseudo-image (b), where the vertical axis denotes the time. In this pseudo-image the membrane is clearly visible. Due to membrane movements, the position of the membrane is not constant in time. These instabilities can be corrected for by shifting each line scan in such a way that the membrane becomes a straight line (c). For each scan, membrane contributions are added up to give one point in the intensity trace (d) which can then be used to calculate the auto-correlation curve $G(\tau)$ (e). (f, g) Geometry of dual-colour and dual-focus scanning FCS.

5. Dual-colour dual-focus scanning fluorescence correlation spectroscopy (FCS)

The implementation of simultaneous dual-colour dual-focus FCS requires only a minor extension of the dual-focus FCS setups for measurements in bulk (3D) solution [9, 34]. Here, however, we demonstrate the feasibility of dual-colour dual-focus FCS by using a scanning FCS approach on spherical model membranes.

5.1. Scanning FCS

Scanning FCS (SFCS) [10] is a powerful extension of FCS that allows the measurement of membrane dynamics not affected by membrane movements. The principle of scanning FCS is illustrated in figure 3. The detection volume is repeatedly scanned perpendicularly through a vertical membrane. The individual line scans can be arranged as a pseudo-image (figure 3(b)), where the vertical axis denotes the time. In this pseudo-image the membrane is clearly visible. Due to instabilities, the position of the membrane is not constant in time. These instabilities can be corrected for by shifting each line scan in such a way that the membrane becomes a straight line. For each scan, membrane contributions are added up to give one point in the intensity $F(t)$, which can then be used to calculate the auto-correlation curve $\tilde{G}(\tau)$ (1). By integrating only the membrane contributions in the shifted pseudo-image instead of summing up the whole line scan, the background is minimized.

In membranes, binding can be measured with dual-colour scanning FCS using two spectral channels. By scanning every other line with a different colour and detecting the photons only in the corresponding channel, the contributions from the two different fluorophores can be separated completely and spectral cross-talk is avoided [10, 20, 21]. This is equivalent to alternating excitation.

For calibration-free diffusion and concentration measurements in membranes, dual-focus scanning FCS can be employed. Here, two parallel lines in a well-defined distance d are

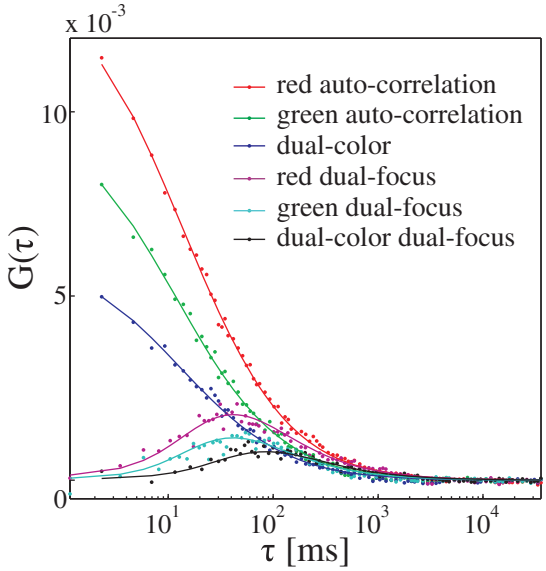

Figure 4. Dual-colour dual-focus scanning FCS on double-labelled DNA bound to a giant unilamellar vesicle composed of DOPC:cholesterol (molar ratio 1 : 1) and 1% DOTAP. Results from the fit: $C_r = 40\,\mu m^{-2}$, $C_g = 125\,\mu m^{-2}$, $C_{rg} = 100\,\mu m^{-2}$, $D = 2.17\,\mu m^2\,s^{-1}$, $d_{rg} = 0.15\,\mu m$. Measurement time= 20 min.

alternatingly scanned through the membrane; the intersections of the scans with the membrane define two detection areas from which two intensity signals can be extracted.

For simultaneous dual-colour dual-focus scanning FCS two spectral excitation and detection channels are used while scanning the two lines [15].

Scanning FCS with the extensions presented above can be easily implemented using a laser scanning microscope (LSM). The use of highly sensitive single-photon detectors (APDs) is recommended since it leads to significantly improved signal-to-noise ratios.

The time resolution of scanning FCS is determined by the repetition rate of the scan and is about 1 ms. This is sufficient to monitor the rather slow diffusion in membranes, but does not capture free solution diffusion or photophysical dynamics (triplet, blinking).

5.2. Quantitative measurement of labelling efficiency on model membranes

Figure 4 shows the result from a dual-colour dual-focus scanning FCS measurement on double-labelled DNA bound to a giant unilamellar vesicle (GUV). It is eminent from the figure that 100% cross-correlation is not achieved, in agreement with dual-colour FCS measurements on the same DNA in solution (data not shown). However, from the solution measurement it is difficult to determine whether the reduced cross-correlation stems from an imperfect overlap of the detection volumes or is a result of incomplete labelling of the DNA. The dual-colour dual-focus scanning FCS measurements, on the other hand, can answer this question, since the spatial overlap of the detection volumes and the absolute concentrations of the red, the green and the double-labelled molecules are free fitting parameters. From the simultaneous fit of all correlation curves it becomes apparent that less than half of the DNA molecules carry both a bright red and a bright green fluorophore. The chromatic aberrations lead to an axial

displacement of the green and red detection volumes of only $d_{rg} = 0.15\,\mu$m. This is much less than their vertical extension and therefore cannot account for the decrease in cross-correlation. Repeated measurements on 5 GUVs yielded similar results: the fraction of double-labelled molecules $38 \pm 8\%$, $D = 2.25 \pm 0.34\,\mu\text{m}\,\text{s}^{-1}$ and $d_{rg} = 0.17 \pm 0.15\,\mu$m.

6. Materials and methods

6.1. Preparation of giant unilamellar vesicles

Giant unilamellar vesicles were produced by a modified electroformation method as described previously [35], using a custom-made closed perfusion chamber heated to 65 °C and indium-tin-oxide-coated coverslips as electrodes. Briefly, a 5 ml lipid mixture (1,2-dioleoyl-*sn*-glycero-3-phosphocholine (DOPC) and cholesterol in the molar ratio 1 : 1 and 1% 1-oleoyl-2-[6-[(7-nitro-2-1,3-benzoxadiazol-4-yl)amino]hexanoyl]-3-trimethylammonium propane (DOTAP), Avanti Polar Lipids) was deposited on indium-tin-oxide-coated coverslips. After evaporation of the solvent, the chamber was assembled and filled with water. A voltage of 1.2 V at 10 Hz was applied for 2 h. Then 1 pmol of short DNA, labelled with Cy5 and Alexa488 (IBA, Goettingen, Germany), was added and measurements were made in the perfusion chamber.

6.2. Dual-colour dual-focus scanning FCS

We performed scanning FCS measurements [10] at 22 °C on an LSM Meta 510 system (Carl Zeiss) using a 40× NA 1.2 UV-vis-IR C Apochromat water-immersion objective, the 488 nm line of an argon-ion laser (25 μW), 633 nm HeNe laser (15 μW) and a home-built detection unit at the fiber output channel. We used a dichroic mirror and band-pass filters (D555, HQ530/60 and HQ700/75; AHF Analyse Technik) behind a collimating achromat to split the emission for the dual-colour detection and to reject residual laser and background light and achromats (LINOS Photonics) to image the internal pinhole onto the apertures of the fibres connected to the APD (PerkinElmer). The photon arrival times were recorded in the photon mode of the hardware correlator Flex 02-01D (correlator.com, Bridgewater, NJ).

We repeatedly scanned the detection volume perpendicularly through the equator of a GUV and controlled its movement directly with Zeiss LSM operation software. The frame mode with $N \times 2$ pixels was used to scan the two parallel lines. We calibrated their distance $d = 0.56\,\mu$m by repeatedly scanning over a film of dried fluorophores and measuring the distance between the bleached traces in a high-resolution LSM image. Practical values are $d = w_0, \ldots, 3w_0$; for larger d the spatial correlation curves become too noisy. Data analysis was performed with software written in MATLAB (MathWorks). The photon stream was binned in bins of 2 μs and arranged as a matrix such that every row corresponded to one line scan. Movements of the membrane were corrected for by calculating the position of the maximum of a running average over several hundreds of line scans and shifting it to the same column. We fitted an average over all rows with a Gaussian and we added only the elements of each row between -2.5σ and 2.5σ to construct the intensity trace. The auto- and cross-correlation curves were computed from the resulting intensity traces with a multiple tau correlation algorithm and fitted with a nonlinear least-squares fitting algorithm. In all FCS data processing, we excluded from further analysis irregular curves resulting from major instabilities and identified by distortions of the curves and a systematic change in the intensity trace.

7. Conclusion

The use of dual-colour FCS to study binding in biological samples has so far been limited by numerous experimental complexities. The mathematical framework and the corrections presented in this work help us to overcome these complexities and extend the use of FCS to experimentally challenging systems. Its implementation in commercial FCS instruments will allow the growing community of FCS users to reduce artefacts and increase the accuracy of FCS.

In particular, the combination of dual-colour FCS with dual-focus FCS bears great potential since it allows quantitative binding studies without the difficult calibration of the overlap of the red and green detection volumes. The implementation of dual-colour dual-focus scanning FCS presented here allows binding measurements on biological membranes; the limited time resolution, however, does not permit its application to quickly diffusing molecules in solution. On the other hand, existing implementations of static dual-focus FCS [9, 34] can be easily extended to dual-colour dual-focus FCS.

Acknowledgment

This work was supported by an HFSP network grant (050503-50) and the Max-Planck-Society (PS fellowship).

Appendix A. Derivation of dual-colour dual-focus correlation functions

In combined dual-colour dual-focus FCS, the intensity fluctuations in four channels are evaluated: the red and the green channel at position 1 and the red and the green channel at position 2 at a distance d from position 1. Here we treat all molecules as non-interacting particles. Therefore, a bound complex is counted as a separate species i. This is possible if the dissociation time is much longer than the diffusion time: $1/k_{\mathrm{off}} \gg \tau_{\mathrm{D}}$.

The intensity $F_k(t)$ in the channel $k = \{r^1, r^2, g^1, g^2\}$ is

$$F_k(t) = \sum_i \eta_{i,k} \int W_k(\mathbf{r}) C_i(\mathbf{r}, t)\, \mathrm{d}^3\mathbf{r}, \tag{A.1}$$

where C_i is the average concentration of species i and $\eta_{i,k}$ is the 'channel brightness' of species i in channel k. Normalization of the molecule detection function to unity $\int W_k(\mathbf{r})\, \mathrm{d}^3\mathbf{r} = 1$ leads to a simple expression for the average intensity:

$$\langle F_k \rangle = \sum_i \eta_{i,k} C_i. \tag{A.2}$$

Note that the channel brightnesses $\eta_{i,k}$ are defined via (A.2) and incorporate also geometric parameters. The usually used molecular brightness $q_{i,k}$ (in cpps) can be calculated after defining a detection volume V_{eff} via $q_{i,k} = \eta_{i,k}/V_{\mathrm{eff}}$.

The normalized cross-correlation function between channels k and l for a stationary system is defined here as

$$G_{kl}(\tau) = \frac{\langle \delta F_k(t) \delta F_l(t+\tau) \rangle}{\langle F_k(t) \rangle \langle F_l(t) \rangle} = \frac{g_{kl}(\tau)}{\langle F_k(t) \rangle \langle F_l(t) \rangle}, \tag{A.3}$$

where $\langle f(t)\rangle = \frac{1}{T}\int_0^T f(t)\,\mathrm{d}t$ denotes the time average over t with the measurement time T, $\delta F(t) = F(t) - \langle F(t)\rangle$ are the fluorescence fluctuations, and $g_{kl}(\tau)$ is the non-normalized correlation function. The auto-correlation functions are obtained by setting $k = l$.

$g_{kl}(\tau)$ can be calculated with the help of the concentration correlation function $\phi_i(\mathbf{r}, \mathbf{r}', \tau)$ for species i and the molecule detection functions $W_k(\mathbf{r})$ and $W_l(\mathbf{r})$ of the two channels [7]:

$$g_{kl} = \sum_i \eta_{i,k}\eta_{i,l}C_i h^{\mathrm{i}}_{\mathrm{kl}}. \tag{A.4}$$

Here we introduced the diffusional part of the correlation function:

$$h^{\mathrm{i}}_{\mathrm{kl}} = \int\int \mathrm{d}^3\mathbf{r}\,\mathrm{d}^3\mathbf{r}'\,\mathrm{W_k}(\mathbf{r})\phi_{\mathrm{i}}(\mathbf{r}, \mathbf{r}', \tau)\mathrm{W_l}(\mathbf{r}'). \tag{A.5}$$

For 3D diffusion the concentration correlation function is

$$\phi_i(\mathbf{r}, \mathbf{r}', \tau) = \frac{1}{(4\pi D\tau)^{3/2}}\exp\left[-\frac{(\mathbf{r}-\mathbf{r}')^2}{4D_i\tau}\right], \tag{A.6}$$

where D_i is the diffusion coefficient of species i.

Usually, a Gaussian molecule detection function is assumed. In three dimensions it reads

$$W_k(x, y, z) = \frac{2^{3/2}}{\pi^{3/2}w^3 S}\exp\left[-2\frac{(x-x_0)^2+(y-y_0)^2}{w^2} - 2\frac{(z-z_0)^2}{S^2w^2}\right], \tag{A.7}$$

where w is the lateral dimension of the Gaussian profile, $S = w_z/w$ is the aspect ratio (structure parameter) and x_0, y_0 and z_0 are its positions. More accurate models [9] can be easily incorporated, but the resulting correlation functions have to be evaluated numerically.

In the following we incorporate the channel brightness η_{r} of the red molecule a in the red channel, the channel brightness η_{g} of the green molecule b in the green channel and the concentration C_i in the definition of the single species correlation functions, $g^{\mathrm{i}}_{\mathrm{rg}} = \eta_{\mathrm{r}}\eta_{\mathrm{g}}C_i h^{\mathrm{i}}_{\mathrm{rg}}$. This leads to the following expression for $g^{\mathrm{i}}_{\mathrm{rg}}$ between the red detection volume at position 1 and the green volume at position 2:

$$g^{\mathrm{i}}_{\mathrm{rg}} = \eta_{\mathrm{r}}\eta_{\mathrm{g}}C_i\frac{2^{3/2}\exp\left[-\frac{2d^2_{\mathrm{rg}}}{8D_i\tau+S^2_{\mathrm{r}}w^2_{\mathrm{r}}+S^2_{\mathrm{g}}w^2_{\mathrm{g}}} - \frac{2d^2}{8D_i\tau+w^2_{\mathrm{r}}+w^2_{\mathrm{g}}}\right]}{\pi^{3/2}\left(8D_i\tau + w^2_{\mathrm{r}} + w^2_{\mathrm{g}}\right)\left(8D_i\tau + S^2_{\mathrm{r}}w^2_{\mathrm{r}} + S^2_{\mathrm{g}}w^2_{\mathrm{g}}\right)^{1/2}}, \tag{A.8}$$

d_{rg} is the displacement between the red and the green detection volume in the z-direction, usually due to chromatic aberrations. Chromatic displacements in the x- or y-direction are less common and are neglected here. d is the lateral distance between foci 1 and 2, which is usually well known in dual-focus experiments and is assumed to have the same value for the red and the green channel. From (A.8) we can obtain the single-colour dual-focus cross-correlation functions by replacing r with g or replacing g with r. Then $d_{\mathrm{rg}} = 0$. The dual-colour cross-correlation functions are obtained by setting $d = 0$. In this way, we can calculate all the necessary correlation functions.

For 2D diffusion in the xz-plane

$$\phi_i(\mathbf{r}, \mathbf{r}', \tau) = \frac{1}{(4\pi D\tau)}\exp\left[-\frac{(\mathbf{r}-\mathbf{r}')^2}{4D_i\tau}\right] \tag{A.9}$$

and

$$W_k(y, z) = \frac{2}{\pi S w^2}\exp\left[-2\frac{(y-d_y)^2}{w^2} - 2\frac{(z-d_z)^2}{S^2w^2}\right], \tag{A.10}$$

which leads to

$$g_{\mathrm{rg}}^{\mathrm{i}} = \eta_{\mathrm{r}}\eta_{\mathrm{g}}C_i \frac{2\exp\left[-\frac{2d_{\mathrm{rg}}^2}{8D_i\tau+S_{\mathrm{r}}^2w_{\mathrm{r}}^2+S_{\mathrm{g}}^2w_{\mathrm{g}}^2} - \frac{2d^2}{8D_i\tau+w_{\mathrm{r}}^2+w_{\mathrm{g}}^2}\right]}{\pi\left(8D_i\tau+w_{\mathrm{r}}^2+w_{\mathrm{g}}^2\right)^{1/2}\left(8D_i\tau+S_{\mathrm{r}}^2w_{\mathrm{r}}^2+S_g^2w_{\mathrm{g}}^2\right)^{1/2}}. \tag{A.11}$$

In the case of 1 : 1 binding of a red molecule a and a green molecule b to form the complex ab we have to consider three species and $i = \{a, b, ab\}$. Using (A.4) we arrive at the expressions for the auto- and cross-correlation functions:

$$\begin{aligned} &\text{single colour} \quad g_{\mathrm{rr}} = g_{\mathrm{rr}}^{\mathrm{a}} + g_{\mathrm{rr}}^{\mathrm{ab}}, \quad g_{\mathrm{gg}} = g_{\mathrm{gg}}^{\mathrm{b}} + g_{\mathrm{gg}}^{\mathrm{ab}}, \\ &\text{dual colour} \quad g_{\mathrm{rg}} = g_{\mathrm{rg}}^{\mathrm{ab}}. \end{aligned} \tag{A.12}$$

The normalized correlation functions can be calculated using the measured average intensities F_{r} and F_{g} as

$$G_{\mathrm{rg}} = \frac{g_{\mathrm{rg}}}{F_{\mathrm{r}}F_{\mathrm{g}}}. \tag{A.13}$$

This equation is valid for single- and dual-focus correlation functions if the corresponding expressions for $g_{\mathrm{rg}}^{\mathrm{i}}$ are used (A.8).

Appendix B. Spectral cross-talk

In the case of spectral cross-talk, the green molecule b contributes to the red intensity. Its brightness in the red channel is $\eta_{\mathrm{b,r}} = \kappa\eta_{\mathrm{g}}$. The cross-talk coefficient κ can be easily inferred using a green-only sample (background B_{r} and B_{g} in red and green channels, respectively) as

$$\kappa = \frac{\langle F_{\mathrm{r}}\rangle - B_{\mathrm{r}}}{\langle F_{\mathrm{g}}\rangle - B_{\mathrm{g}}}. \tag{B.1}$$

The intensity in the channels is

$$\begin{aligned} F_{\mathrm{r}} &= \eta_{\mathrm{r}}(C_{\mathrm{a}} + C_{\mathrm{ab}}) + \kappa\eta_{\mathrm{g}}(C_{\mathrm{b}} + C_{\mathrm{ab}}), \\ F_{\mathrm{g}} &= \eta_{\mathrm{r}}(C_{\mathrm{b}} + C_{\mathrm{ab}}). \end{aligned} \tag{B.2}$$

Usually, the size and position of the detection volume are defined by the excitation. Therefore, the experimental auto- and cross-correlation curves are equal in the case of only green fluorophores in the sample. Then the correlation functions are given by (6):

$$\begin{aligned} g_{\mathrm{rr}} &= g_{\mathrm{rr}}^{\mathrm{a}} + g_{\mathrm{rr}}^{\mathrm{ab}} + \kappa^2 g_{\mathrm{gg}}^{\mathrm{b}} + \kappa^2 g_{\mathrm{gg}}^{\mathrm{ab}} + 2\kappa g_{\mathrm{rg}}^{\mathrm{ab}}, \\ g_{\mathrm{rg}} &= g_{\mathrm{rg}}^{\mathrm{ab}} + \kappa g_{\mathrm{gg}}^{\mathrm{b}} + \kappa g_{\mathrm{gg}}^{\mathrm{ab}}, \\ g_{\mathrm{gg}} &= g_{\mathrm{gg}}^{\mathrm{b}} + g_{\mathrm{gg}}^{\mathrm{ab}}. \end{aligned} \tag{B.3}$$

When fitting the correlation curves, η_{r} and η_{g} have to be expressed using the measured average intensities F_{r} and F_{g} and the the concentrations C_{a}, C_{b} and C_{ab} (fitting parameters):

$$\eta_{\mathrm{r}} = \frac{F_{\mathrm{r}} - \kappa F_{\mathrm{g}}}{C_{\mathrm{a}} + C_{\mathrm{ab}}}, \quad \eta_{\mathrm{g}} = \frac{F_{\mathrm{g}}}{C_{\mathrm{b}} + C_{\mathrm{ab}}}. \tag{B.4}$$

When additionally cross-talk from the red fluorophore into the green channel is present, it can be taken into account in the same way [22].

Appendix C. Incomplete or statistical labelling, spectral cross-talk and multiple binding sites

In general, A molecules of species a, carrying together K red fluorophores, can form complexes with B molecules of species b, carrying in total L fluorophores. Then we have to take into account all species K, L, A, B with concentrations C_{AB}^{KL}.

The number of fluorophores K on one monomer of species a varies statistically and is described by the probability distribution $p(K)$. The distribution for molecule b is $p(L)$.

For simplicity, we assume that all aggregates can be approximately described by the same diffusion coefficient D_{ab}. The complex formation is described by the probability $p(A, B)$, which in general does not factorize (e.g. 2 receptors + 2 ligands form a complex: $p(2, 2) = 1$). We separate the case $(A = 1,\ B = 0)$, $(A = 0,\ B = 1)$ (monomers of species a, b) from the complexes ab and do not include these cases in the definition of the probability distribution (because of their different diffusion coefficients D).

$$C_{10}^{K0} = p(K)C_{\mathrm{a}}, \quad C_{01}^{0L} = p(L)C_{\mathrm{b}}, \quad C_{AB}^{KL} = p(A, B, K, L)C_{\mathrm{ab}}. \tag{C.1}$$

For the joint probability distribution describing the probability of complexes with A, B molecules with K, L fluorophores, we can write

$$p(K, L, A, B) = p(A, B)p(K|A)p(L|B). \tag{C.2}$$

The brightness of a molecule with K, L fluorophores is

$$\eta_{K,r} = \eta_{\mathrm{r}}K, \quad \eta_{L,r} = \eta_{\mathrm{g}}\kappa L, \quad \eta_{L,g} = \eta_{\mathrm{g}}L. \tag{C.3}$$

As in appendix B, $\kappa{=}\eta_{b,r}/\eta_{b,g}$.

The average intensities in the green and red channels are

$$\begin{aligned} F_{\mathrm{g}} &= \sum_{L} \eta_{\mathrm{g}}Lp(L)C_{\mathrm{b}} + \sum_{A,B}\sum_{K,L} \eta_{\mathrm{g}}Lp(A, B)p(K|A)p(L|B)C_{\mathrm{ab}} \\ &= \eta_{\mathrm{g}}\bar{L}C_{\mathrm{b}} + \eta_{\mathrm{g}} \sum_{A,B} p(A, B) \sum_{L} Lp(L|B)C_{\mathrm{ab}} \\ &= \eta_{\mathrm{g}}\bar{L}C_{\mathrm{b}} + \eta_{\mathrm{g}} \sum_{A,B} p(A, B)B\bar{L}C_{\mathrm{ab}} \\ &= \eta_{\mathrm{g}}\bar{L}C_{\mathrm{b}} + \eta_{\mathrm{g}}\bar{B}\bar{L}C_{\mathrm{ab}}, \end{aligned} \tag{C.4}$$

$$\begin{aligned} F_{\mathrm{r}} &= \sum_{K} \eta_{\mathrm{r}}Kp(K)C_{\mathrm{a}} + \sum_{A,B}\sum_{K,L} \eta_{\mathrm{r}}Kp(A, B)p(K|A)p(L|B)C_{\mathrm{ab}} \\ &\quad + \sum_{L} \eta_{\mathrm{g}}\kappa Lp(L)C_{\mathrm{b}} + \sum_{A,B}\sum_{K,L} \eta_{\mathrm{g}}\kappa Lp(A, B)p(K|A)p(L|B)C_{\mathrm{ab}} \\ &= \eta_{\mathrm{r}}\bar{K}C_{\mathrm{a}} + \eta_{\mathrm{g}}\kappa\bar{L}C_{\mathrm{b}} + \sum_{A,B} p(A, B)\eta_{\mathrm{r}}A\bar{K}C_{\mathrm{ab}} + \sum_{A,B} p(A, B)\eta_{\mathrm{g}}\kappa B\bar{L}C_{\mathrm{ab}} \\ &= \eta_{\mathrm{r}}\bar{K}C_{\mathrm{a}} + \eta_{\mathrm{g}}\kappa\bar{L}C_{\mathrm{b}} + \left(\eta_{\mathrm{r}}\bar{A}\bar{K} + \eta_{\mathrm{g}}\kappa\bar{B}\bar{L}\right)C_{\mathrm{ab}}, \end{aligned} \tag{C.5}$$

$\bar{K} = \sum_{K} Kp(K)$ is the mean value (first moment) of the distribution $p(K)$, and $\bar{A} = \sum_{A,B} Ap(A, B)$ is the first moment of $p(A, B)$.

Non-normalized correlation functions can be calculated as follows:

$$
\begin{aligned}
g_{\mathrm{rr}} &= \sum_K K^2 p(K) g_{\mathrm{rr}}^{\mathrm{a}} + \sum_L \kappa^2 L^2 p(L) g_{\mathrm{gg}}^{\mathrm{b}} \\
&\quad + \sum_{A,B} \sum_{K,L} K^2 p(A,B) p(K|A) p(L|B) g_{\mathrm{rr}}^{\mathrm{ab}} \\
&\quad + \sum_{A,B} \sum_{K,L} \kappa^2 L^2 p(A,B) p(K|A) p(L|B) g_{\mathrm{gg}}^{\mathrm{ab}} \\
&\quad + 2 \sum_{A,B} \sum_{K,L} \kappa K L p(A,B) p(K|A) p(L|B) g_{\mathrm{gr}}^{\mathrm{ab}} \\
&= \overline{K^2}\, g_{\mathrm{rr}}^{\mathrm{a}} + \kappa^2 \overline{L^2}\, g_{\mathrm{gg}}^{\mathrm{b}} \\
&\quad + \sum_{A,B} p(A,B) \Bigg(\sum_K K^2 p(K|A) \sum_L p(L|B) g_{\mathrm{rr}}^{\mathrm{ab}} \\
&\quad + \kappa^2 \sum_K p(K|A) \sum_L L^2 p(L|B) g_{\mathrm{gg}}^{\mathrm{ab}} \\
&\quad + 2\kappa \sum_K K p(K|A) \sum_L L p(L|B) g_{\mathrm{gr}}^{\mathrm{ab}} \Bigg) \\
&= \overline{K^2}\, g_{\mathrm{rr}}^{\mathrm{a}} + \kappa^2 \overline{L^2}\, g_{\mathrm{gg}}^{\mathrm{b}} + \sum_{A,B} p(A,B)((A\,\overline{K^2} + A(A-1)\bar{K}^2) g_{\mathrm{rr}}^{\mathrm{ab}} \\
&\quad + \kappa^2 (B\,\overline{L^2} + B(B-1)\bar{L}^2) g_{\mathrm{gg}}^{\mathrm{ab}} + 2\kappa AB \bar{K}\bar{L} g_{\mathrm{rg}}^{\mathrm{ab}}) \\
&= \overline{K^2}\, g_{\mathrm{rr}}^{\mathrm{a}} + \kappa^2 \overline{L^2}\, g_{\mathrm{gg}}^{\mathrm{b}} + (\bar{A}\,\overline{K^2} + (\overline{A^2} - \bar{A})\bar{K}^2) g_{\mathrm{rr}}^{\mathrm{ab}} \\
&\quad + \kappa^2 (\bar{B}\,\overline{L^2} + (\overline{B^2} - \bar{B})\bar{L}^2) g_{\mathrm{gg}}^{\mathrm{ab}} + 2\kappa\, \overline{AB}\, \bar{K}\bar{L} g_{\mathrm{rg}}^{\mathrm{ab}}.
\end{aligned}
\tag{C.6}
$$

In a similar way, we can calculate

$$
\begin{aligned}
g_{\mathrm{rg}} &= \sum_{A,B} \sum_{K,L} K L p(A,B) p(K|A) p(L|B) g_{\mathrm{rg}}^{\mathrm{ab}} \\
&\quad + \sum_{A,B} \sum_{K,L} \kappa L^2 p(A,B) p(K|A) p(L|B) g_{\mathrm{gg}}^{\mathrm{ab}} + \sum_L \kappa L^2 p(L) g_{\mathrm{gg}}^{\mathrm{b}} \\
&= \overline{AB}\, \bar{K}\bar{L} g_{\mathrm{rg}}^{\mathrm{ab}} + \kappa (\bar{B}\,\overline{L^2} + (\overline{B^2} - \bar{B})\bar{L}^2) g_{\mathrm{gg}}^{\mathrm{ab}} + \kappa\, \overline{L^2}\, g_{\mathrm{gg}}^{\mathrm{b}}
\end{aligned}
\tag{C.7}
$$

$$
g_{\mathrm{gg}} = \overline{L^2}\, g_{\mathrm{gg}}^{\mathrm{b}} + (\bar{B}\,\overline{L^2} + (\overline{B^2} - \bar{B})\bar{L}^2) g_{\mathrm{gg}}^{\mathrm{ab}}. \tag{C.8}
$$

Moments of distributions used here are:
Definitions of moments:

$$
\sum_K K p(K) \equiv \bar{K}, \tag{C.9}
$$

$$
\sum_K K^2 p(K) \equiv \overline{K^2}, \tag{C.10}
$$

$$\sum_{A,B} Ap(A,B) \equiv \bar{A}, \tag{C.11}$$

$$\sum_{A,B} A^2 p(A,B) \equiv \overline{A^2}, \tag{C.12}$$

$$\sum_{A,B} ABp(A,B) \equiv \overline{AB}. \tag{C.13}$$

Derived expressions:

$$\sum_{K} Kp(K|A) = A\bar{K}, \tag{C.14}$$

$$\sum_{K} K^2 p(K|A) = A\,\overline{K^2} + A(A-1)\bar{K}^2, \tag{C.15}$$

$$\sum_{K} p(K|A) = 1. \tag{C.16}$$

Proofs for (C.14):

$$\begin{aligned}\sum_{K} Kp(K|A) &= \sum_{K_1 \ldots K_A} \left(\sum_{i=1}^{A} K_i\right) \prod_i p(K_i) = A \sum_{K_1 \ldots K_A} K_1 \prod_i p(K_i) \\ &= A \sum_{K_1} K_1 p(K_1) = A\bar{K}.\end{aligned} \tag{C.17}$$

The sum over all realizations of total K labels on A molecules is written as the sum of all combinations of K_i labels ($i = 1 \ldots A$) on A molecules; $K = \sum_{i=1}^{A} K_i$. The product is the probability of one particular realization of $K_1, K_2, \ldots, K_A$ labels. The numbers of labels on individual molecules are independent; therefore we take only one (K_1) and multiply by A. Sums over $i \neq 1$ give 1. The proof for C.15 is analogous:

$$\begin{aligned}\sum_{K} K^2 p(K|A) &= \sum_{K_1 \ldots K_A} \left(\sum_{i=1}^{A} K_i\right)^2 \prod_i p(K_i) \\ &= \sum_{K_1 \ldots K_A} \left(\sum_i K_i^2 + \sum_{i \neq j} K_i K_j\right) \prod_i p(K_i) \\ &= A\overline{K^2} + A(A-1)\bar{K}^2.\end{aligned} \tag{C.18}$$

Here we considered A pairs with the same index (K_i^2), and $A(A-1)$ pairs with different indices ($K_i K_j$).

This formalism also describes aggregation of only one species a ($B = 0$).

The channel brightness used for fitting is

$$\eta_{\mathrm{r}} = \frac{F_{\mathrm{r}} - \kappa F_{\mathrm{g}}}{\bar{K}(C_{\mathrm{a}} + \bar{A}C_{\mathrm{ab}})}, \quad \eta_{\mathrm{g}} = \frac{F_{\mathrm{g}}}{\bar{L}(C_{\mathrm{b}} + \bar{B}C_{\mathrm{ab}})}. \tag{C.19}$$

Appendix D. Blinking and triplet

Changes of the molecular brightness due to blinking or population of the triplet state are usually taken into account by an additional dynamic term $T(\tau)$:

$$g_t(\tau) = (1 + T(\tau))g(\tau); \quad T(\tau) = \frac{f_T}{1 - f_T} \mathrm{e}^{-\tau/\tau_t}. \tag{D.1}$$

Here $g(\tau)$ denotes the correlation function without triplet or blinking, f_T is the fraction of molecules in the dark state and the triplet/blinking time $\tau_t = (k_{\mathrm{on}} + k_{\mathrm{off}})^{-1}$ is the corresponding timescale.

To investigate the triplet contributions for K fluorophores in one complex, we can sum up the non-normalized correlation functions of the single fluorophores a, b, c, ..., taking into account the correlation between them. The auto-correlation parts g_{a}, g_{b}, ..., exhibit blinking. The cross-correlation terms g_{ab},... correspond to two different fluorophores. Since blinking between them is independent, no blinking term appears here:

$$\begin{aligned} g &= g_{\mathrm{a}} + g_{\mathrm{b}} + g_c + \cdots + g_{\mathrm{ab}} + g_{ba} + g_{ac} + g_{ca} + g_{bc} + g_{ca} + \cdots \\ &= K g^t + K(K-1)g = (K + KT(\tau))g + K(K-1)g = K^2 g + KT(\tau)g. \end{aligned} \tag{D.2}$$

For statistical labelling, only terms in the correlation function stemming from one and the same molecule exhibit a triplet term; cross-correlation terms between different molecules (KL-terms) do not exhibit blinking:

$$\begin{aligned} \sum_K K^2 p(K) g_{\mathrm{rr}}^{\mathrm{i}} \to \sum_K (K^2 + KT(\tau)) p(K) g_{\mathrm{rr}}^{\mathrm{i}} \\ = (\overline{K^2} + \bar{K} T(\tau)) g_{\mathrm{rr}}^{\mathrm{i}}. \end{aligned} \tag{D.3}$$

Therefore, the triplet can be taken into account with a simple substitution:

$$\overline{K^2} \to \overline{K^2}(\tau) = \overline{K^2} + \bar{K} T(\tau). \tag{D.4}$$

(D.4) is valid in general since only auto-correlation terms (K^2, L^2) give rise to second moments ($\overline{K^2}$, $\overline{L^2}$). This holds true even in the case of multiple binding sites, as is shown in the following.

Terms in (C.6) depending only on KL do not show any triplet and result in terms with $\bar{K}\bar{L}$. The quadratic term K^2 with triplet is

$$\begin{aligned} \sum_{A,B} p(A,B) \sum_K K^2 p(K|A) &\to \sum_{A,B} p(A,B) \sum_K (K^2 + KT(\tau)) p(K|A) \\ &= \sum_{A,B} p(A,B) \left(\sum_K K^2 p(K|A) + \sum_K KT(\tau) p(K|A) \right) \\ &= \sum_{A,B} p(A,B)(A\,\overline{K^2} + A(A-1)\bar{K}^2 + A\bar{K}T(\tau)) \\ &= \bar{A}\,\overline{K^2} + (\overline{A^2} - \bar{A})\bar{K}^2 + \bar{A}\bar{K}T(\tau) \\ &= \bar{A}(\overline{K^2} + \bar{K}T(\tau)) + (\overline{A^2} - \bar{A})\bar{K}^2. \end{aligned} \tag{D.5}$$

Comparison with (C.6) without triplet demonstrates the validity of (D.4).

References

[1] Schwille P, Meyer-Almes F J and Rigler R 1997 Dual-color fluorescence cross-correlation spectroscopy for multicomponent diffusional analysis in solution *Biophys. J.* **72** 1878–86

[2] Rigler R and Elson E 2001 *Fluorescence Correlation Spectroscopy: Theory and Applications* (Berlin: Springer)

[3] Bacia K and Schwille P 2003 A dynamic view of cellular processes by in vivo fluorescence auto- and cross-correlation spectroscopy *Methods* **29** 74–85

[4] Bacia K, Kim S A and Schwille P 2006 Fluorescence cross-correlation spectroscopy in living cells *Nature Methods* **3** 83–9

[5] Kim S A, Heinze K G and Schwille P 2007 Fluorescence correlation spectroscopy in living cells *Nature Methods* **4** 963–73

[6] Ries J, Yu S R, Burkhardt M, Brand M and Schwille P 2009 Modular scanning fcs quantifies receptor–ligand interactions in living multicellular organisms *Nature Methods* **6** 643–5

[7] Petrov E P and Schwille P 2008 State of the art and novel trends in fluorescence correlation spectroscopy *Standardization and Quality Assurance in Fluorescence Measurements II (Springer Series on Fluorescence)* vol 6 pp 145–97

[8] Enderlein J, Gregor I, Patra D, Dertinger T and Kaupp U B 2005 Performance of fluorescence correlation spectroscopy for measuring diffusion and concentration *ChemPhysChem* **6** 2324–36

[9] Dertinger T, Pacheco V, von der Hocht I, Hartmann R, Gregor I and Enderlein J 2007 Two-focus fluorescence correlation spectroscopy: a new tool for accurate and absolute diffusion measurements *ChemPhysChem* **8** 433–43

[10] Ries J and Schwille P 2006 Studying slow membrane dynamics with continuous wave scanning fluorescence correlation spectroscopy. *Biophys. J.* **91** 1915–24

[11] Petrášek Z and Schwille P 2008 Precise measurement of diffusion coefficients using scanning fluorescence correlation spectroscopy *Biophys. J.* **94** 1437–48

[12] Wallrabe H and Periasamy A 2005 Imaging protein molecules using FRET and FILM microscopy *Curr. Opin. Biotechnol.* **16** 19–27

[13] Jares-Erijman A E and Jovin T M 2003 FRET imaging *Nature Biotechnol.* **21** 1387–95

[14] Harpur A G, Wouters F S and Bastiaens P I 2001 Imaging FRET between spectrally similar GFP molecules in single cells *Nature Biotechnol.* **19** 167–9

[15] García-Sáez A J, Ries J, Orzáez M, Pérez-Payà E and Schwille P 2009 Membrane promotes tBID interaction with BCLXL *Nature Struct. Mol. Biol.* **16** 1178–85

[16] Digman M A, Brown C M, Sengupta P, Wiseman P W, Horwitz A R and Gratton E 2005 Measuring fast dynamics in solutions and cells with a laser scanning microscope *Biophys. J.* **89** 1317–27

[17] Hebert B, Costantino S and Wiseman P W 2005 Spatiotemporal image correlation spectroscopy (STICS) theory, verification, and application to protein velocity mapping in living CHO cells *Biophys. J.* **88** 3601–14

[18] Bacia K and Schwille P 2007 Practical guidelines for dual-color fluorescence cross-correlation spectroscopy *Nature Protoc.* **2** 2842–56

[19] Maeder C I, Hink M A, Kinkhabwala A, Mayr R, Bastiaens P I H and Knop M 2007 Spatial regulation of FUS3 MAP kinase activity through a reaction-diffusion mechanism in yeast pheromone signalling *Nature Cell. Biol.* **9** 1319–26

[20] Muller B K, Zaychikov E, Brauchle C and Lamb D C 2005 Pulsed interleaved excitation *Biophys. J.* **89** 3508–22

[21] Thews E, Gerken M, Eckert R, Zapfel J, Tietz C and Wrachtrup J 2005 Cross talk free fluorescence cross correlation spectroscopy in live cells *Biophys. J.* **89** 2069–76

[22] Rička J and Binkert T 1989 Direct measurement of a distinct correlation-function by fluorescence cross-correlation *Phys. Rev.* A **39** 2646–52

[23] Petersen N O 1986 Scanning fluorescence correlation spectroscopy. 1. Theory and simulation of aggregation measurements *Biophys. J.* **49** 809–15
[24] Tcherniak A, Reznik C, Link S and Landes C F 2009 Fluorescence correlation spectroscopy: criteria for analysis in complex systems *Anal. Chem.* **81** 746–54
[25] Ries J, Chiantia S and Schwille P 2009 Accurate determination of membrane dynamics with line-scan FCS *Biophys. J.* **96** 1999–2008
[26] Delon A, Usson Y, Derouard J, Biben T and Souchier C 2006 Continuous photobleaching in vesicles and living cells: a measure of diffusion and compartmentation *Biophys. J.* **90** 2548–62
[27] Ries J and Schwille P 2008 New concepts for fluorescence correlation spectroscopy on membranes *Phys. Chem. Chem. Phys.* **10** 3487–97
[28] Petrášek Z and Schwille P 2008 Photobleaching in two-photon scanning fluorescence correlation spectroscopy *ChemPhysChem* **9** 147–58
[29] Banks D S and Fradin C 2005 Anomalous diffusion of proteins due to molecular crowding *Biophys. J.* **89** 2960–71
[30] Nishimura G and Kinjo M 2005 Dead-time distortion in fluorescence correlation measurements *Appl. Opt.* **44** 3458–67
[31] Zhao M, Jin L, Chen B, Ding Y, Ma H and Chen D 2003 Afterpulsing and its correction in fluorescence correlation spectroscopy experiments *Appl. Opt.* **42** 4031–6
[32] Ries J, Bayer M, Csucs G, Dirkx R, Solimena M, Ewers H and Schwille P 2010 Automated suppression of sample-related artifacts in fluorescence correlation spectroscopy *Opt. Express* **18** 11073–82
[33] Skakun V V, Hink M A, Digris A V, Engel R, Novikov E G, Apanasovich V V and Visser A J W G 2005 Global analysis of fluorescence fluctuation data *Euro. Biophys. J.* **34** 323–34
[34] Muller C B, Loman A, Pacheco V, Koberling F, Willbold D, Richtering W and Enderlein J 2008 Precise measurement of diffusion by multi-color dual-focus fluorescence correlation spectroscopy *Europhys. Lett.* **83** 46001
[35] Kahya N, Scherfeld D, Bacia K, Poolman B and Schwille P 2003 Probing lipid mobility of raft-exhibiting model membranes by fluorescence correlation spectroscopy *J. Biol. Chem.* **278** 28109–15